JACS
JOURNAL OF THE AMERICAN CHEMICAL SOCIETY
Article
pubs.acs.org/JACS

Precisely Tunable Engineering of Sub-30 nm Monodisperse Oligonucleotide Nanoparticles

Antons Sizovs,[†] Xianzhou Song,[†] M. Neal Waxham,[⊥] Yilong Jia,[∥] Fude Feng,[†] Jianwei Chen,[†] Amanda C. Wicker,[#] Jianming Xu,[‡] Yan Yu,[∥] and Jin Wang*[,†,§]

[†]Department of Pharmacology, [‡]Department of Molecular and Cellular Biology, [§]Center for Drug Discovery, Dan L. Duncan Cancer Center, and Cardiovascular Research Institute, Baylor College of Medicine, Houston, Texas 77030, United States

[⊥]Department of Neurobiology and Anatomy, University of Texas Health Science Center at Houston, Houston, Texas 77030, United States

[∥]Department of Chemistry, Indiana University, Bloomington, Indiana 47401, United States

[#]Department of Chemistry, Rice University, Houston, Texas 77030, United States

Supporting Information

ABSTRACT: Advancement of RNAi therapies is mainly hindered by the development of efficient delivery vehicles. The ability to create small size (<30 nm) oligonucleotide nanoparticles is essential for many aspects of the delivery process but is often overlooked. In this report, we describe diblock star polymers that can reproducibly complex double-stranded oligonucleotides into monodisperse nanoparticles with 15, 23, or 30 nm in diameter. The polymer−nucleic acid nanoparticles have a core−shell architecture with dense PEG brush coating. We characterized these nanoparticles using ITC, DLS, FRET, FCS, TIRF, and TEM. In addition to small size, these nanoparticles have neutral zeta-potentials, making the presented polymer architecture a very attractive platform for investigation of yet poorly studied polyplex size range for siRNA and antisense oligonucleotide delivery applications.

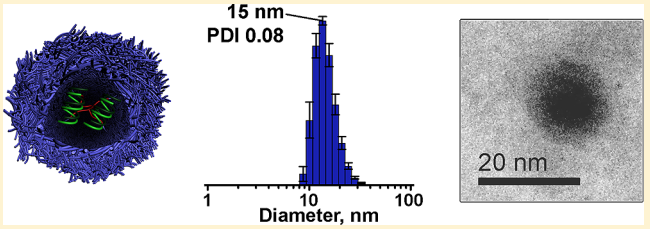

1. INTRODUCTION

The ability to down-regulate genes via RNA interference (RNAi) was reported in 1998, and its great potential as a therapeutic approach, especially for cancer, was quickly recognized.[1] However, delivery of siRNA to the site of interest remains the major roadblock for clinical applications of RNAi therapy.[2,3] Nanoparticles (NPs) hold the promise to solve this long-standing problem. To achieve targeting, NPs should avoid renal filtration and the clearance by the mononuclear phagocyte system.[4−6] Many studies suggested that the size of NPs has a direct correlation with their systemic and intratumoral distribution, and NPs in the size range of 10−30 nm may achieve deeper tumor penetration,[7−12] avoid accelerated blood clearance,[13,14] and be best suited for targeting.[15,16] However, due to the difficulty in controlling organic-based nanoparticle size precisely, the size influence on performance of NPs is still elusive. Cationic polymers are often used to complex siRNA into nanoparticles ("polyplexes") for delivery purpose. However, this process usually leads to polydisperse NPs that typically are above 60 nm in size, more often above 100 nm. PRINT technology developed by DeSimone et al. elegantly solved this long-standing polydispersity problem and is able to produce monodisperse particles for nucleic acid delivery.[17,18] However, the current development of PRINT technology has not yet allowed production of nanoparticles under 50 nm.[19]

Fabrication of ultrasmall (<30 nm) nanoparticles has been realized by a few groups using inorganic particles,[8,9,20−24] polymer and lipid-based particles,[25−33] nucleic acid conjugates,[34,35] or self-assembly into oligonucleotide particles.[36] Most of the polymer-based systems inherently suffer from polydispersity. Fabrication of the nucleic acid nanoparticles with precisely controlled small size and homogeneity is not a trivial task and is rarely addressed in the literature. In this report, we describe core−shell star polymers that can complex 2, 16, and 53 molecules of oligonucleic acid (NA) resulting in nanoparticles with diameters of 15, 23, and 30 nm, respectively. These nanoparticles are monodisperse (polydispersity indexes (PDIs) < 0.08), have neutral zeta-potentials, and are colloidally stable for days in phosphate buffered saline. The formation of these nanoparticles is very straightforward and is accomplished by mixing the star polymers with NA, which is amenable to be quickly adapted by nonexperts in drug delivery. With the great cost reduction of next-generation genomic sequencing and the daunting complexity of patient-dependent tumor environment, personalized medicine is expected to significantly improve the outcome of cancer treatment. Our convenient fabrication method for NA nanoparticles has the potential to take personalized nanomedicine one step closer to being practical.

Received: August 28, 2013
Published: November 27, 2013

   dx.doi.org/10.1021/ja408879b | J. Am. Chem. Soc. 2014, 136, 234−240

We envision that our star polymers may have the potential to serve as a platform for future development of targeted NA delivery to overcome the common problems associated with nanoparticle sizes, heterogeneity, stability, and cancer targeting.

2. RESULTS AND DISCUSSION

2.1. Synthesis and Characterization of Star Polymers.

In this report, we present a strategy based on star polymers with an uncrowded cationic core for hosting NA and dense corona that consists of PEG brush polymers (Figure 1A). We employed reversible addition−fragmentation chain transfer (RAFT) polymerization[37−39] using tetravalent chain transfer agent (CTA) and *N*-(2-aminoethyl) methacrylamide hydrochloride (AEMA·HCl) to synthesize star polymers with four cationic arms (star polymer cores), followed by polymerization of α-methoxy-ω-methacrylamido poly(ethylene glycol) (PEG-MA, M_n = 2 kDa) to obtain final structures (Scheme 1).

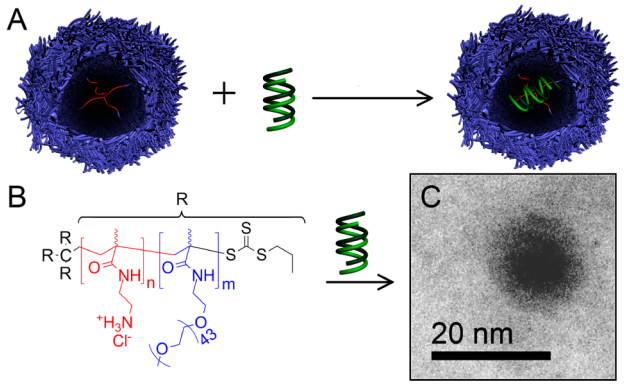

Figure 1. (A) Schematic illustration of nucleic acid (NA) complexation by star polymer. (B) Structure of the star polymers. (C) TEM image of a Star-1/NA nanoparticle with visibly distinguishable polyamine/NA core (black) and PEG polymer brush corona (dark gray).

We started by making per-tosylated pentaerythritol **2**, which was subsequently used to obtain Boc-protected tetraamine **3** that contains thioether linkages. In addition to molecular weight determination by size exclusion chromatography/static light scattering (SEC-SLS), incorporation of the thioether group allowed us to conveniently determine number-averaged molecular weight (M_n) of the first block using NMR (see Supporting Information for more details). Boc groups were then removed, and the produced tetraamine was converted into tetravalent CTA **6** in a reaction with NHS-ester **5**.

Polymerizations of AEMA·HCl were conducted at 70 °C in deoxygenated DMSO using 4,4′-(diazene-1,2-diyl)bis(4-cyanopentanoic acid) (V-501) as initiator and CTA **6** to yield three star polymers (cationic cores) with degrees of polymerization (DP) of 14, 31, and 47 per arm (Table 1). These polymers were purified by dialysis against ultrapure water, lyophilized, and used as macroCTAs in the polymerization of PEG-MA. Chain extension with PEG-MA was conducted in a similar fashion, using a water/DMSO mixture as a solvent and V-501 as initiator (see Supporting Information for details). Star polymers were purified by dialysis and finally lyophilized to yield desired materials.

Polymers were analyzed by SEC-SLS, NMR, UV−Vis, and dynamic light scattering (DLS) (see Table 1 for summary and

Scheme 1. Synthesis of Tetravalent Chain Transfer Agent and Star Polymers

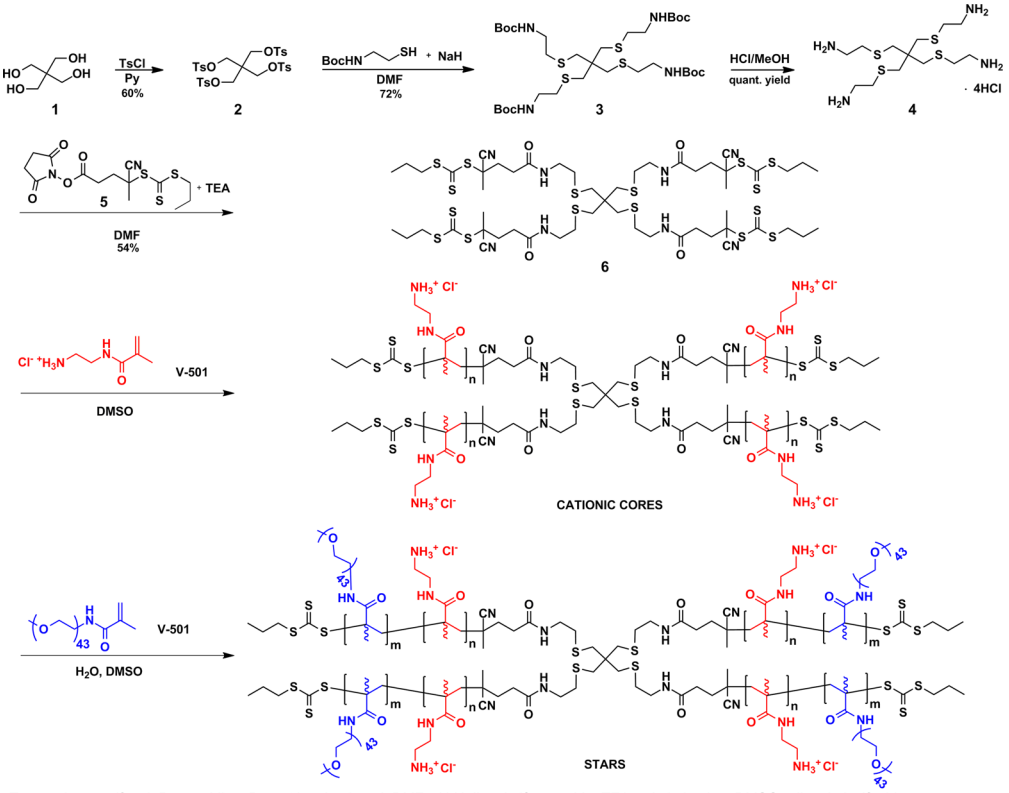

Ts - *p*-toluenesulfonyl, Py - pyridine, Boc - *t*-butylcarbonyl, DMF - *N*,*N*-dimethylformamide, TEA - triethylamine, DMSO - dimethylsulfoxide
V-501 - 4,4'-(diazene-1,2-diyl)bis(4-cyanopentanoic acid)

dx.doi.org/10.1021/ja408879b | J. Am. Chem. Soc. 2014, 136, 234−240

Table 1. Physical Characterization of Star Polymers by Size Exclusion Chromatography/Static Light Scattering and Dynamic Light Scattering

	cationic cores				core−shell stars			DLS	
polymer	M_w (kDa)	M_n (kDa)	PDI (M_w/M_n)	DP	M_w (kDa)	M_n (kDa)	PDI (M_w/M_n)	D_H	PDI
Star-1	9.71	9.52	1.03	14	188.8	144.7	1.31	11	0.084
Star-2	21.9	21.5	1.02	31	328.3	229.9	1.43	13	0.083
Star-3	33.8	32.5	1.04	47	227.1	178.8	1.27	12	0.078

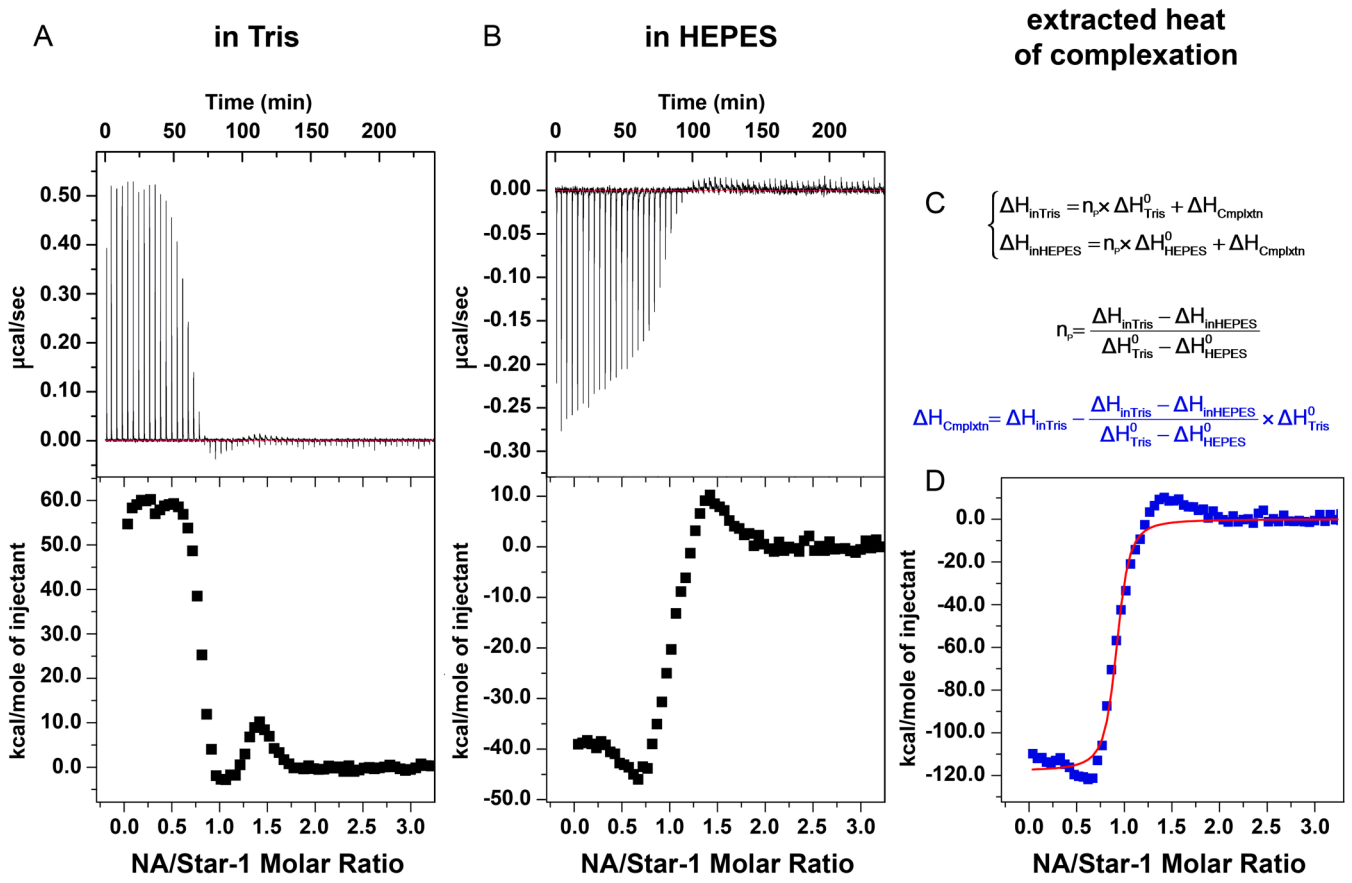

Figure 2. Isothermal titration calorimetry (ITC). (A) Star-1 titration with dsDNA in Tris buffer. (B) Star-1 titration with dsDNA in HEPES buffer. (C) Calculation of the heat of complexation based on titrations in two buffers for each data point. (D) Extracted heat of complexation of dsDNA by Star-1 polymer.

Supporting Information for details). AEMA·HCl polymerization resulted in polymers with expected molecular weights and narrow polydispersity indexes (PDIs < 1.04). Number-averaged molecular weights (M_n) obtained by SEC matched those obtained by the end-group analysis using ^{1}H-NMR. Polymerization of PEG-MA was less controlled and resulted in final structures with PDIs ranging from 1.27 to 1.43. The slight loss of the control can be attributed to the bulky nature of the PEG-MA monomer and even bulkier nature of the propagating PEG bottle brush chain; therefore, elevated PDIs were expected. Dense PEG coating, however, is essential for good antifouling properties and resistance to opsonization and bulky nature of the resulting brush is crucial for controlling the self-assembly; therefore, use of high molecular weight PEG was necessary.

2.2. Calorimetric Analysis of the Complexation Processes of Star Polymers and Nucleic Acids. To investigate the ability of star polymers to complex NA, we performed isothermal titration calorimetry (ITC) measurements. Since the goal for this paper is to establish a fabrication method for small NA nanoparticles, we focus our studies on 22 base-pair double-stranded DNA (dsDNA) for cost-effective reasons. Because the complexation process between dsDNA and the star polymers is driven by charge−charge interactions, we expect that dsDNA would be a reasonable surrogate for siRNA in this report. Star-1 will be taken as an example to demonstrate our analysis of the ITC data. In the ITC experiments, dsDNA and the star polymer were dissolved in the same buffer and dsDNA was titrated into the star polymer solution at 37 °C.

The apparent heat produced during the complexation is a result of two processes: (1) heat of the complexation between dsDNA and the star polymer ($\Delta H_{cmplxtn}$) and (2) heat of neutralization of n_p moles of protons released by buffer ($n_p\Delta H^\circ_{buffer}$). In order to obtain the pure heat of complexation $\Delta H_{cmplxtn}$ without the contribution from the buffer neutralization process, we conducted titrations in two buffers, namely, Tris and HEPES both at pH 7.4 (Figure 2A,B; see Supporting Information for experimental details). By solving a system of linear equations in two variables for each injection, where

dx.doi.org/10.1021/ja408879b | J. Am. Chem. Soc. 2014, 136, 234−240

$\Delta H_{\text{in Tris}}$ and $\Delta H_{\text{in HEPES}}$ are apparent heats measured by ITC and $\Delta H^{\circ}_{\text{Tris}}$ and $\Delta H^{\circ}_{\text{HEPES}}$ are standard heats of neutralization equal to 11.33 and 4.87 kcal·mol^{-1}, respectively,[40] we extracted the heat of complexation $\Delta H_{\text{cmplxtn}}$ between the star polymers and NA (Figure 2C; see Supporting Information for a calculation example). Overall, the complexation process was found to be enthalpy-driven, similar to the previously reported polyamine/NA binding (e.g., PAMAM).[41] Interestingly, there were two separate equilibria observed. One of them is strongly exothermic and defines the overall negative enthalpy of the complexation process. On the contrary, the second accompanying process is endothermic, which can be concluded from the positive heats observed beyond 1.25 equiv of added NA, and is driven by entropy (Figure 2D). Based on the established composition for Star-1/NA nanoparticle (vide infra), the two equilibria are

$$\text{Star-1} + \text{NA} \rightleftharpoons \text{Star-1/NA} \quad K_1$$

$$2\ \text{Star-1/NA} \rightleftharpoons (\text{Star-1/NA})_2 \quad K_2$$

At this point, we were unable to obtain separate values for K_1 and K_2 as both equilibria overlap. We used a one-site binding model to fit the data, which cannot distinguish between two equilibria; however, it allowed us to obtain the number of NA equivalents that is incorporated into nanoparticles and get an estimate of the overall order of binding ($K = K_1 \times K_2$, Table 2).

Table 2. Summary of Isothermal Titration Calorimetry Results

polymer	NA (equiv)	ΔH (kcal·mol^{-1})	K (M^{-1})
Star-1	0.9	−112 ± 2	10^8
Star-2	1.9	−133 ± 4	10^7
Star-3	3.7	−155 ± 2	10^7

We used heats produced during the initial injections to obtain the enthalpy values.[42,43] As shown in Table 2, the enthalpy increases with the increase in size of the cationic core, which suggests that the polymer with the largest core undergoes greater conformational changes to maximize charge−charge interactions compared to a star polymer with a smaller core. In addition, because two separate processes can be observed with ITC and the Star-1 nanoparticle has a known composition, this system is an interesting model to study the polymer/nucleic acid complexation process in detail and will be reported in a separate investigation.

2.3. Hydrodynamic Diameters and Surface Charges. We formulated nanoparticles using the equivalence values obtained from the ITC experiments and determined their sizes with DLS. All three polymers, Star-1, Star-2, and Star-3, produced monodisperse particles with 15, 23, and 30 nm in hydrodynamic diameter, respectively (Figure 3). Particle fabrication is highly reproducible, as evident from the small standard deviation values (Figure 3C). Importantly, no change in particle hydrodynamic diameters was observed for all three nanoparticles over a 7 day time period, attesting to their colloidal stability (Figure 3B; see Supporting Information for histograms). It is interesting to note that all three star polymers have similar hydrodynamic diameters (Table 1), but the sizes of the corresponding nanoparticles increase with the increase in the size of the star polymer cores. In a free, uncomplexed state, the star polymer core exists in a relaxed conformation; however, upon complexation of the rigid NA, the cationic core may

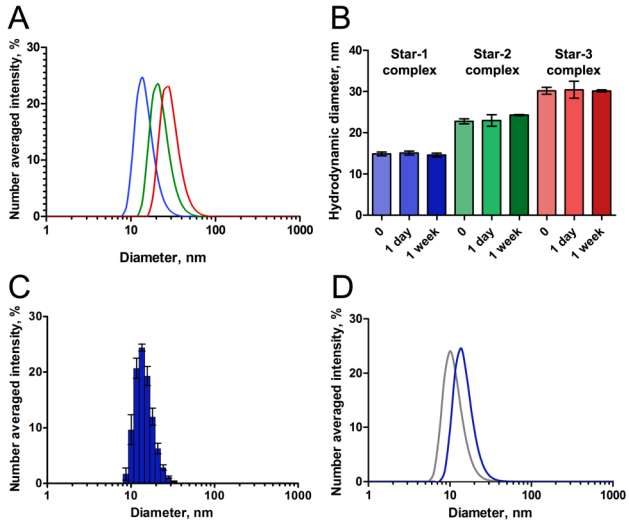

E

Polymer	Polymer, D_H, nm	Polymer PDI	NA (eq)	Complex, D_H, nm	Complex PDI
Star-1	11	0.084	1	15	0.078
Star-2	13	0.083	2	23	0.084
Star-3	12	0.078	3.7	30	0.083

Figure 3. DLS analysis of polymers and nanoparticles. (A) Histograms of NA nanoparticles formed by Star-1 (blue), Star-2 (green), and Star-3 (red). (B) Hydrodynamic diameters of nanoparticles over time in phosphate buffered saline. Star-1 (blue), Star-2 (green), and Star-3 (red). Error bars represent SD of three formulations. (C) Histogram of Star-1/NA nanoparticle. Error bars represent SD of three formulations. (D) Comparison of the traces between Star-1 polymer (gray) and Star-1 nanoparticle (blue). (E) Hydrodynamic diameters of polymers and corresponding nanoparticles at time 0.

adopt a more extended conformation to maximize enthalpic gain from the electrostatic interactions. As the steric bulk possessed by the PEG brush is moved farther away from the star polymer focal point with an increase in cationic core size, it enables the accommodation of more polymer molecules inside the nanoparticle (vide infra).[44]

Zeta-potential measurements of NA nanoparticles resulted in neutral zeta-potentials; however, it should be noted that the quality of the zeta-potential measurements was suboptimal even when nanoparticles were formulated using high concentration NA solution (150 μM; see Supporting Information for details). This is understandable as the electrophoretic mobility becomes indistinguishable from the Brownian motion at neutral zeta-potential. Neutral zeta-potential is another property desired for delivery applications as it helps to avoid nonspecific interactions with biological molecules and cells.[45]

2.4. Determination of the Composition of Nanoparticles. Recently, the groups of Radler and Chen independently reported single siRNA nanoparticles, which have hydrodynamic diameters of 30 and 25 nm, respectively.[31,33] We were curious to know how many NA molecules there are in our smallest nanoparticle derived from Star-1 (D_H = 15 nm). In addition, it was predicted by Wittrup et al. that the size of an IgG immunoglobulin (~15 nm) is the optimal size for systemic targeting,[16] which balances renal filtration and tumor tissue penetration. Therefore, nanoparticles derived from polymer Star-1 possess a special interest as a platform for NA delivery.

Star-1/NA nanoparticle was visualized using transmission electron microscopy (TEM) with uranyl acetate staining. As

dx.doi.org/10.1021/ja408879b | J. Am. Chem. Soc. 2014, 136, 234−240

shown in Figure 4, Star-1/NA nanoparticles reveal spherical shapes and uniform distribution. The diameter obtained by

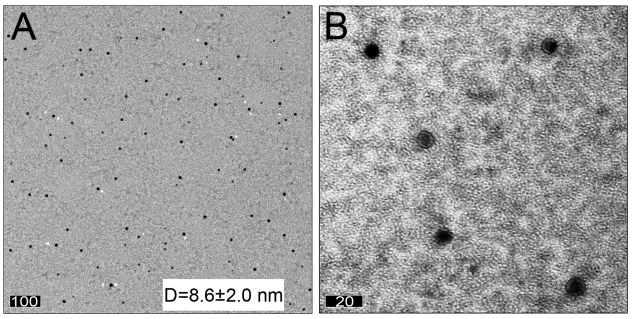

Figure 4. Characterization of Star-1 nanoparticles. (A) TEM image of Star-1/NA nanoparticle stained with uranyl acetate. Scale bar equals 100 nm. Average diameter ± SD was calculated with ImageJ software by analysis of 112 particles. (B) Close-up TEM image of Star-1/NA nanoparticles. Scale bar equals 20 nm. PEG brush corona can be observed as an under-stained ring surrounding a polyamine/NA core.

TEM is 8.6 ± 2.0 nm based on the analysis of more than 100 nanoparticles. It is smaller than the hydrodynamic diameter obtained by DLS in part due to the sample preparation (drying) and poor staining of the PEG brush by uranyl acetate (as opposed to the complexed NA that stains well). The poor staining of the PEG brush, however, allowed us to observe a distinct core and corona (Figures 1C and 4B), revealing the desired core−shell architecture of the particle with PEG corona coating the polyplex.

The hydrodynamic diameter of the Star-1/NA nanoparticle is only 4 nm greater than the hydrodynamic diameter of the polymer itself, and the uniform size distribution remains virtually unchanged (Figure 3D,E). Additionally, the size of the core as evident by TEM is less than 10 nm, which was used previously as an argument by Chen et al.[31] to conclude the presence of only one NA molecule in the complex. To test if this hypothesis stands in the case of our system, we prepared nanoparticles between Star-1 polymer and a mixture of equal amounts of Cy3-labeled oligo and Cy5-labeled oligo (*Note*: all the dye-labeled dsDNA oligos used in the following experiments were HPLC-purified and contain only one dye molecule per oligo). When a solution of this nanoparticle was excited at 520 nm, a significant increase in fluorescence at 665 nm and decrease in fluorescence at 565 nm was observed (Figure 5, blue trace) compared to the negative control—solution of oligos alone at the same total oligo concentration (Figure 5, black trace). This change in fluorescence is a result of Förster resonance energy transfer (FRET) between two oligos, and it indicates that complexation with Star-1 brings oligos with two different dyes together; thus the nanoparticles derived from Star-1 contain *at least* two oligos per particle.

This result motivated us to determine the exact number of NA molecules in nanoparticles, which was accomplished using fluorescence correlation spectroscopy (FCS) measurements. Similar to DLS for nonfluorescent species, FCS measures the intensity fluctuation of the fluorescent species in order to determine the diffusion coefficients and the number of fluorescent species in a fixed small volume. The number of fluorescently labeled NA molecules per nanoparticle can be calculated based on the change in a number of the fluorescent species upon complexation.[33,46] Figure 6A shows the autocorrelation curves for Alexa-488 dsDNA oligo solution at

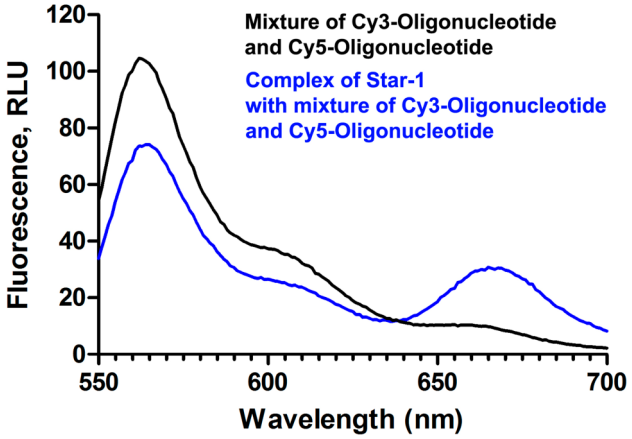

Figure 5. Observation of FRET in Star-1-derived nanoparticles. A decrease in Cy-3 fluorescence and an increase in Cy-5 fluorescence is observed when mixture of Cy-3 and Cy-5 labeled oligos is complexed by Star-1 polymer. 520 nm excitation wavelength was used to directly excite Cy-3 dye but not Cy-5.

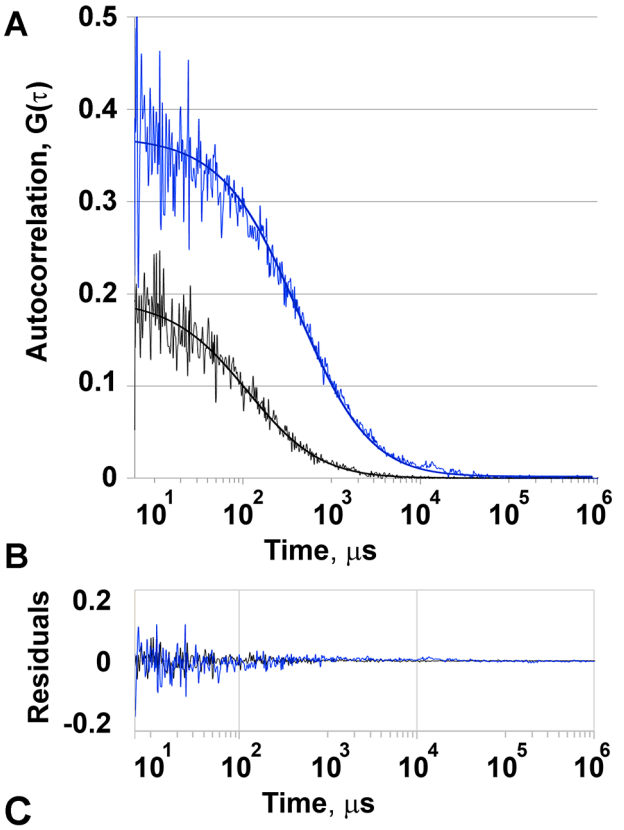

C

Nanoparticle	D_H, nm	PDI	#NA/NP	#polymers/NP
Star-1 NP	15	0.078	2	2
Star-2 NP	23	0.084	16	8
Star-3 NP	30	0.083	53	15

Figure 6. (A) Correlation functions of Alexa-488−dsDNA oligo (black) and its nanoparticle with Star-1 polymer (blue). Both measurements were conducted at 40 nM oligo concentration. Best fits with monoexponential decay are represented by solid lines. (B) Residuals from the fits for Alexa-488−dsDNA oligo (black) and its nanoparticle with Star-1 polymer (blue). (C) Number of oligos per particle (#NA/NP) and number of polymers per particle (#polymer/NP). D_H and PDI were obtained with DLS measurements.

dx.doi.org/10.1021/ja408879b | *J. Am. Chem. Soc.* 2014, 136, 234−240

40 nM (black) and the solution of its nanoparticle with Star-1 at the same oligo concentration (blue). Solid lines represent the best fits with monoexponential decays, and the residuals for these fits are shown in Figure 6B. The number of the observed fluorescent species is inversely proportional to the intercept of the autocorrelation function fit with the *y*-axis. As shown in Figure 6A, the number of fluorescent species decreased 2-fold, indicating that there are two oligonucleotide molecules in each Star-1/NA nanoparticle. In a similar fashion, we have analyzed the nanoparticles formed with Star-2 and Star-3 polymers (Figure 6C; see Supporting Information for more details). Thus, eight molecules of Star-2 polymer assemble into nanoparticles that contain 16 molecules of oligo, while the Star-3 polymer, which has the steric bulk of PEG brush moved the farthest away from the star polymer focal point, assembles in NPs that contains 14 polymer molecules and 53 molecules of oligo.

In addition, the smallest nanoparticle was also analyzed by total internal reflection fluorescence (TIRF) microscopy using the stepwise single-molecule photobleaching method as previously described.[47] When nanoparticles containing dsDNA oligos that are labeled with Cy-5 were continuously illuminated with the laser, individual Cy-5 molecules photobleached stochastically and the total number of photobleaching steps indicated the number of dsDNA-Cy5 in a particular nanoparticle. Fluorescence images (Figure 7A) show a

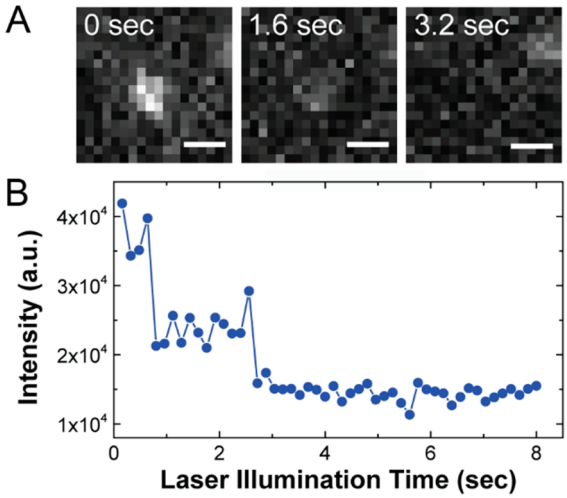

Figure 7. Stepwise single-molecule photobleaching of Star-1/Cy-5NA complex. (A) TIRF images of a representative particle undergoing photobleaching after continuous laser illumination of indicated times. Scale bars: 500 nm. (B) Fluorescence intensity of the particle shown in panel A is plotted as a function of laser illumination time, showing a two-step photobleaching profile.

representative nanoparticle undergoing a two-step photobleaching process, which is evident in its corresponding integral fluorescence intensity versus time plot (Figure 7B). The result indicates that the photobleached nanoparticle contains two Cy5-dsDNAs. We found, by analyzing approximately 600 particles, that Star-1 polymer complexes with 1.7 ± 0.8 dsDNAs on average.

2.5. In Vitro Toxicity of NA Nanoparticles. In addition to the desired physical properties, nanoparticles must be nontoxic in order to serve as a platform for oligonucleotide delivery. We evaluated the viability of HeLa cells incubated with various concentrations of the nanoparticles using MTT assay. As shown in Figure 8, cell viability remained unchanged when cells were exposed to nanoparticles at up to 100 μg/mL (concentrations

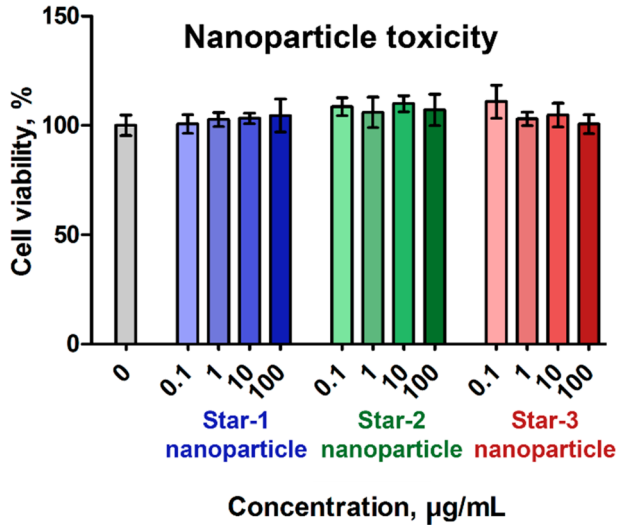

Figure 8. Viability of HeLa cells upon 24 h incubation with nanoparticles at various concentrations. Error bars represent standard deviation between six wells.

shown based on polymer concentration). This concentration corresponds to 0.7 and 2.1 μM of NA in the case of Star-1 and Star-3 nanoparticles, respectively, which is significantly higher than the NA concentrations used for delivery applications. In addition, no cell morphology changes were observed (data not shown) at all the concentrations tested, supporting the results of the MTT assay.

3. CONCLUSIONS

In conclusion, the investigations of the polymer-based oligonucleotide delivery vehicles in a particularly attractive size range (<30 nm) have been hindered by difficulties in obtaining particles of these sizes. Herein, we reported star polymers with architecture that allows us to form such particles, which are small, have low polydispersity and neutral zeta-potentials, and are colloidally stable. The fabrication of these nanoparticles is simple and highly reproducible, and the size of nanoparticles can be controlled within the 15−30 nm range. Neither polymers nor derived nanoparticles have any appreciable cellular toxicity. In addition, trithiocarbonate groups available on the distal side of these polymers (and nanoparticles) are excellent handles for decorating the nanoparticles with targeting ligands. Consequently, these star polymers will serve as a great platform for future explorations in applications of oligonucleotide delivery.

■ ASSOCIATED CONTENT

Supporting Information

Experimental details on synthesis, ITC, DLS, FRET, FCS, TIRF, and in vitro toxicity. This material is available free of charge via the Internet at http://pubs.acs.org.

■ AUTHOR INFORMATION

Corresponding Author

wangj@bcm.edu

Notes

The authors declare no competing financial interest.

dx.doi.org/10.1021/ja408879b | *J. Am. Chem. Soc.* 2014, 136, 234−240

■ ACKNOWLEDGMENTS

This work is supported in part by the Cancer Prevention and Research Institute of Texas (CPRIT R1104), the Welch Foundation (Q-1798), the Cardiovascular Research Institute (CVRI) at Baylor College of Medicine, the Caroline Wiess Law Fund for Research in Molecular Medicine, the Curtis Hankamer Basic Research Fund and the ARCO Foundation Young Teacher-Investigator Award to J.W., the Extreme Science and Engineering Discovery Environment (XSEDE), the Center for Drug Discovery at Baylor College of Medicine, the Integrated Microscopy Core at Baylor College of Medicine with funding from the NIH (HD007495, DK56338, and CA125123), the Dan L. Duncan Cancer Center, the John S. Dunn Gulf Coast Consortium for Chemical Genomics, and the Shared Equipment Authority instrumentation at Rice University. M.N.W. would like to acknowledge an endowment from the William Wheless III Professorship. F.F. would like to acknowledge the CPRIT fellowship. The authors also would like to thank Drs. Joseph DeSimone, Dar-Chone Chow, and Yuhong Wang for insightful discussions.

■ REFERENCES

(1) Fire, A.; Xu, S.; Montgomery, M. K.; Kostas, S. A.; Driver, S. E.; Mello, C. C. *Nature* **1998**, *391*, 806−11.
(2) Whitehead, K. A.; Langer, R.; Anderson, D. G. *Nat. Rev. Drug Discovery* **2009**, *8*, 129−38.
(3) Kesharwani, P.; Gajbhiye, V.; Jain, N. K. *Biomaterials* **2012**, *33*, 7138−50.
(4) Peer, D.; Karp, J. M.; Hong, S.; Farokhzad, O. C.; Margalit, R.; Langer, R. *Nat. Nanotechnol.* **2007**, *2*, 751−60.
(5) Davis, M. E.; Chen, Z. G.; Shin, D. M. *Nat. Rev. Drug Discovery* **2008**, *7*, 771−82.
(6) Longmire, M.; Choyke, P. L.; Kobayashi, H. *Nanomedicine* **2008**, *3*, 703−17.
(7) Lee, H.; Fonge, H.; Hoang, B.; Reilly, R. M.; Allen, C. *Mol. Pharmaceutics* **2010**, *7*, 1195−208.
(8) Tang, L.; Fan, T. M.; Borst, L. B.; Cheng, J. *ACS Nano* **2012**, *6*, 3954−66.
(9) Tang, L.; Gabrielson, N. P.; Uckun, F. M.; Fan, T. M.; Cheng, J. *Mol. Pharmacol.* **2013**, *10*, 883−92.
(10) Kawai, M.; Higuchi, H.; Takeda, M.; Kobayashi, Y.; Ohuchi, N. *Breast Cancer Res.* **2009**, *11*, R43.
(11) Cabral, H.; Matsumoto, Y.; Mizuno, K.; Chen, Q.; Murakami, M.; Kimura, M.; Terada, Y.; Kano, M. R.; Miyazono, K.; Uesaka, M.; Nishiyama, N.; Kataoka, K. *Nat. Nanotechnol.* **2011**, *6*, 815−23.
(12) Perrault, S. D.; Walkey, C.; Jennings, T.; Fischer, H. C.; Chan, W. C. W. *Nano Lett.* **2009**, *9*, 1909−15.
(13) Koide, H.; Asai, T.; Kato, H.; Ando, H.; Shiraishi, K.; Yokoyama, M.; Oku, N. *Int. J. Pharm.* **2012**, *432*, 75−9.
(14) Koide, H.; Asai, T.; Hatanaka, K.; Urakami, T.; Ishii, T.; Kenjo, E.; Nishihara, M.; Yokoyama, M.; Ishida, T.; Kiwada, H.; Oku, N. *Int. J. Pharm.* **2008**, *362*, 197−200.
(15) Schmidt, M. M.; Wittrup, K. D. *Mol. Cancer Ther.* **2009**, *8*, 2861−71.
(16) Wittrup, K. D.; Thurber, G. M.; Schmidt, M. M.; Rhoden, J. J. *Methods Enzymol.* **2012**, *503*, 255−68.
(17) Dunn, S. S.; Tian, S.; Blake, S.; Wang, J.; Galloway, A. L.; Murphy, A.; Pohlhaus, P. D.; Rolland, J. P.; Napier, M. E.; DeSimone, J. M. *J. Am. Chem. Soc.* **2012**, *134*, 7423−30.
(18) Xu, J.; Wang, J.; Luft, J. C.; Tian, S.; Owens, G.; Pandya, A. A.; Berglund, P.; Pohlhaus, P.; Maynor, B. W.; Smith, J.; Hubby, B.; Napier, M. E.; DeSimone, J. M. *J. Am. Chem. Soc.* **2012**, *134*, 8774−7.
(19) Personal communication.
(20) Rosi, N. L.; Giljohann, D. A.; Thaxton, C. S.; Lytton-Jean, A. K. R.; Han, M. S.; Mirkin, C. A. *Science* **2006**, *312*, 1027−30.
(21) Cutler, J. I.; Auyeung, E.; Mirkin, C. A. *J. Am. Chem. Soc.* **2012**, *134*, 1376−91.
(22) Zheng, D.; Giljohann, D. A.; Chen, D. L.; Massich, M. D.; Wang, X.-Q.; Iordanov, H.; Mirkin, C. A.; Paller, A. S. *Proc. Natl. Acad. Sci. U.S.A.* **2012**, *109*, 11975−80.
(23) Zhang, K.; Hao, L.; Hurst, S. J.; Mirkin, C. A. *J. Am. Chem. Soc.* **2012**, *134*, 16488−91.
(24) Li, J.; Yang, Y.; Huang, L. *J. Controlled Release* **2012**, *158*, 108−14.
(25) Lee, V. Y.; Havenstrite, K.; Tjio, M.; McNeil, M.; Blau, H. M.; Miller, R. D.; Sly, J. *Adv. Mater.* **2011**, *23*, 4509−15.
(26) Cho, H. Y.; Srinivasan, A.; Hong, J.; Hsu, E.; Liu, S.; Shrivats, A.; Kwak, D.; Bohaty, A. K.; Paik, H.-J.; Hollinger, J. O.; Matyjaszewski, K. *Biomacromolecules* **2011**, *12*, 3478−86.
(27) Cho, H. Y.; Averick, S. E.; Paredes, E.; Wegner, K.; Averick, A.; Jurga, S.; Das, S. R.; Matyjaszewski, K. *Biomacromolecules* **2013**, *14*, 1262−7.
(28) Li, A.; Luehmann, H. P.; Sun, G.; Samarajeewa, S.; Zou, J.; Zhang, S.; Zhang, F.; Welch, M. J.; Liu, Y.; Wooley, K. L. *ACS Nano* **2012**, *6*, 8970−82.
(29) Shrestha, R.; Elsabahy, M.; Florez-Malaver, S.; Samarajeewa, S.; Wooley, K. L. *Biomaterials* **2012**, *33*, 8557−68.
(30) Zhang, S.; Zou, J.; Zhang, F.; Elsabahy, M.; Felder, S. E.; Zhu, J.; Pochan, D. J.; Wooley, K. L. *J. Am. Chem. Soc.* **2012**, *134*, 18467−74.
(31) Yan, M.; Liang, M.; Wen, J.; Liu, Y.; Lu, Y.; Chen, I. S. Y. *J. Am. Chem. Soc.* **2012**, *134*, 13542−5.
(32) Derouchey, J.; Schmidt, C.; Walker, G. F.; Koch, C.; Plank, C.; Wagner, E.; Rädler, J. O. *Biomacromolecules* **2008**, *9*, 724−32.
(33) Rudorf, S.; Rädler, J. O. *J. Am. Chem. Soc.* **2012**, *134*, 11652−8.
(34) Jeong, J. H.; Mok, H.; Oh, Y.-K.; Park, T. G. *Bioconjugate Chem.* **2009**, *20*, 5−14.
(35) Rozema, D. B.; Lewis, D. L.; Wakefield, D. H.; Wong, S. C.; Klein, J. J.; Roesch, P. L.; Bertin, S. L.; Reppen, T. W.; Chu, Q.; Blokhin, A. V; Hagstrom, J. E.; Wolff, J. A. *Proc. Natl. Acad. Sci. U.S.A.* **2007**, *104*, 12982−7.
(36) Lee, H.; Lytton-Jean, A. K. R.; Chen, Y.; Love, K. T.; Park, A. I.; Karagiannis, E. D.; Sehgal, A.; Querbes, W.; Zurenko, C. S.; Jayaraman, M.; Peng, C. G.; Charisse, K.; Borodovsky, A.; Manoharan, M.; Donahoe, J. S.; Truelove, J.; Nahrendorf, M.; Langer, R.; Anderson, D. G. *Nat. Nanotechnol.* **2012**, *7*, 389−93.
(37) Moad, G.; Rizzardo, E.; Thang, S. H. *Aust. J. Chem.* **2006**, *59*, 669.
(38) Moad, G.; Rizzardo, E.; Thang, S. H. *Aust. J. Chem.* **2009**, *62*, 1402.
(39) Moad, G.; Rizzardo, E.; Thang, S. H. *Aust. J. Chem.* **2012**, *65*, 985.
(40) Goldberg, R. N. *J. Phys. Chem. Ref. Data* **1999**, *31*, 231.
(41) Jensen, L. B.; Mortensen, K.; Pavan, G. M.; Kasimova, M. R.; Jensen, D. K.; Gadzhyeva, V.; Nielsen, H. M.; Foged, C. *Biomacromolecules* **2010**, *11*, 3571−7.
(42) Braun, C. S.; Vetro, J. A.; Tomalia, D. A.; Koe, G. S.; Koe, J. G.; Middaugh, C. R. *J. Pharm. Sci.* **2005**, *94*, 423−36.
(43) Jensen, L. B.; Pavan, G. M.; Kasimova, M. R.; Rutherford, S.; Danani, A.; Nielsen, H. M.; Foged, C. *Int. J. Pharm.* **2011**, *416*, 410−8.
(44) Raviña, M.; de la Fuente, M.; Correa, J.; Sousa-Herves, A.; Pinto, J.; Fernandez-Megia, E.; Riguera, R.; Sanchez, A.; Alonso, M. J. *Macromolecules* **2010**, *43*, 6953−6961.
(45) Alexis, F.; Pridgen, E.; Molnar, L. K.; Farokhzad, O. C. *Mol. Pharmaceutics* **2008**, *5*, 505−15.
(46) DeRouchey, J.; Walker, G. F.; Wagner, E.; Rädler, J. O. *J. Phys. Chem. B* **2006**, *110*, 4548−54.
(47) Das, S. K.; Darshi, M.; Cheley, S.; Wallace, M. I.; Bayley, H. *ChemBioChem* **2007**, *8*, 994−9.